



By Francesco Di Caprio¹, Valerio Acanfora², Stefania Franchitti¹, Rosario Borrelli¹, Aniello Riccio²
 1. CIRA – Italian Aerospace Research Center - 2. Department of Engineering, University of Campania “L. Vanvitelli”

Numerical applications of an Ansys-based tool to analyze hybrid metal/composite lattice structures

Computationally efficient method enables design and optimization processes of axial-symmetric lattice structures to be conducted simply and quickly

This paper, by means of presenting three application cases, provides a brief description of the capabilities of a numerical tool developed for the design and optimization of hybrid metal/composite lattice structures created with 3D printing. The tool allows a large number of axial symmetrical structures to be generated in the ANSYS environment through the use of a macro written in APDL language. The models generated can be used for both sensitivity analyses and structural optimization processes (they are totally parametrized). The strength of the procedure is its ability to generate many unit cells by defining a matrix structure that activates specific connectivity flags. The models generated are not too expensive computationally due both to the simplification of the models (made with beam and shell elements) and to the elimination of any possible multiple point constraints (MPC) elements between the nodes of the lattice structure and the remaining solid parts. This enables the finite element (FE) models generated to also be used for more expensive analyses such as non-linear buckling ones.

Additive manufacturing (AM) has projected the global industry into a new phase of transformation in product design and fabrication. This change involves both the manufacturing and research fields in

a radical way. Indeed, the use of AM is increasing rapidly in many industrial sectors [1- 4]. The reason for this success is based on the fact that 3D printing technology uses a particular and elegant methodology known as additive layering. Specifically, this additive methodology allows an object to be created layer by layer, in a totally different way from the subtractive techniques commonly used. It enables the construction of complex geometries and easily makes use of a wide variety of materials. The preliminary phase of AM is based on a computer-aided design (CAD) of the object to be realized [5-7]. This is where the construction of elaborate shapes, for instance lattice or porous structures, is simplified, or organic constructions are generated with topological optimization [8,9]. Furthermore, the costs of the wastage of resulting materials are significantly reduced with additive technology, compared to the subtractive technique. In fact, Additive Manufacturing makes it possible to “print” a prototype by only stratifying the regions required by the CAD model with material. [10,11].

Thanks to these advantages, AM can be widely adopted in a rapidly changing sector like aerospace. The necessity to develop strategies to reduce fuel consumption and manufacturing costs and times is one of the main objectives of aerospace research. This also all leads to the significant use of hybrid metal/composite structures.

■ CASE STUDIES

Among these hybrid combinations, the coupling of carbon fiber reinforced polymer (CFRP) composite materials with titanium alloys is the most suitable for aerospace use due to the similarities of the thermal expansion coefficients (a highly relevant aspect for composite manufacturing processes) of these materials. In addition, this characteristic reduces the issues related to galvanic corrosion.

The increasing demand for hybrid components characterized by complex shapes and high performance requires both the numerical design tools and the manufacturing processes to be upgraded. The present study presents some numerical applications of an innovative numerical design tool [12] developed for the preliminary design and numerical investigation of hybrid structures made, mainly, from a lattice structure. The developed routine allows modelling in an FE environment and the structural optimization of hybrid composite/lattice metal structures with different shapes and loading conditions. More specifically, the structures analyzed were considered to have been manufactured with Electron Beam Melting (EBM) technology for the metallic parts, and filament winding for the composite parts. In particular, the tool is dedicated to the design of axial symmetric components.

For the numerical implementation of the lattice part, there are many methodologies in the literature [13-15] that are based on tetrahedral cells in a repetitive configuration. Usually, however, these are unable to adjust to the outer borders (the cell edges are cut from the edges of the structure). Other methods, developed in commercial codes, can create other types of unitary cell structures (cubic, octahedral, etc. [16-20]), but even these are unable to adapt to complex geometries. Instead, this routine, developed in APDL, is able to overcome these limits because it allows any type of unit cell to be generated, and to be adapted if the user desires, to any type of frontier in an axial symmetrical structure. The algorithm to generate the internal lattices is very efficient, simple to manage and does not require significant computational power.

Description of the proposed routine

The routine [12] presented in this work has been developed in APDL and tested in Ansys 16.1 and later.

As indicated in Fig. 1, the procedure consists of 12 main parts:

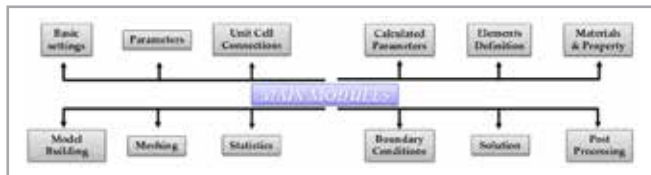


Fig. 1 - Main modules of the routine

The initial stage of the macro requires Basic Settings to be defined. In this phase, the user selects the desired graphics options, the file name, and the resolution of the images that will be generated during the execution of the procedure. The second stage concerns the definition of all the parameters and options to allow the geometric models to be generated, and the definition of all parameters related

to the required analysis. In addition, to ensure consistent design, automated parameter checking is implemented to minimize the possibility of creating non-generable geometries.

The third and most critical module concerns the definition of the connections between the nodes of the Unit Cell (UC). It is possible to create two different Unit Cell architectures: an 8-node Unit Cell, and a 27-node Unit Cell (Fig. 3). The connection between the nodes is defined by activating a flag (1 or 0). In the fourth module (Calculated Parameters), additional parameters to correctly dimension the UC are assessed by combining all the previously defined parameters.

The fifth and sixth modules aim to define the element type and the mechanical properties of the selected materials. Another particularly delicate phase of the routine is that dedicated to the construction of the model. In this seventh module, it is possible to generate any type of hybrid axial symmetric structure, regardless of its geometric complexity. Fig. 2 shows some examples of the types of structures it is possible to realize.

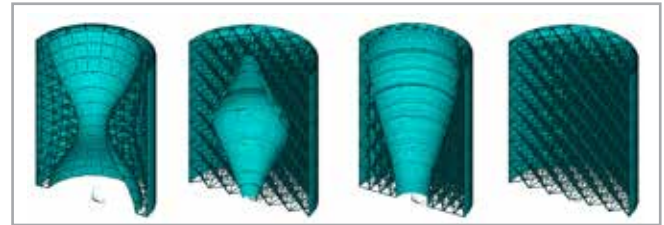


Fig. 2 - Examples of possible structures

In the eighth part of the routine, the structural mesh is generated, while the Statistics section evaluates some important data (total mass, mass and volume of each part, FE details). The last three modules of the procedure concern the boundary conditions to be applied, the type of analysis to be carried out, and the generation of the constraint and objective functions for the optimization phase, respectively. The routine offers the possibility of running different types of analyses: a linear structural analysis, a non-linear static analysis (non-linear buckling), and a linear buckling analysis.

Unit cell definition

A significant part of the routine being presented is the Unit Cell design, which is used to generate the entire lattice structure. Different families of

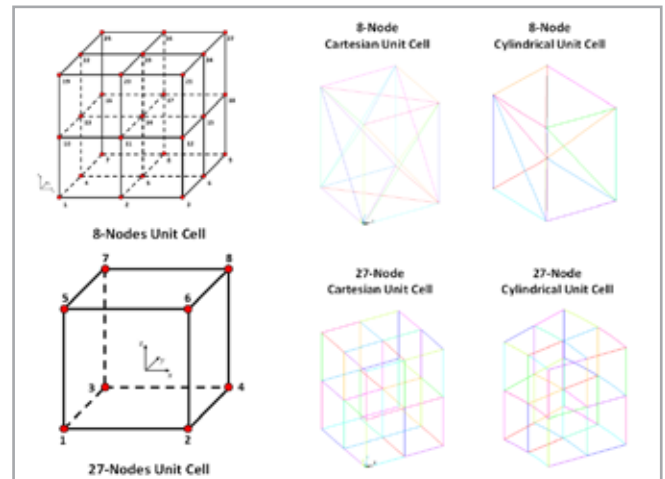


Fig. 3 - Unit Cell classification

unit cells have been developed for the design of the metallic lattice parts. A first classification is based on the number of nodes (no FE entities) of the unit cell. Two options are available: unit cells with 8 nodes or unit cells with 27 nodes (Fig. 3). In addition, by combining cells with 27 and 8 nodes, it is possible to realize unit cells with more than 27 nodes. Depending on the type of construction reference system being used to generate the unit cells, it is possible to obtain a second classification: unit cells with a quadrangular prism-based structure, or cylindrical sectors (Fig. 3).

Cylindrical unit cells provide additional functionalities:

- Straight or curved beams. This option allows a perfect integration of the lattice regions in axial symmetric structures.
- Bias factor. By activating the bias factor, the cells will increase in size as they move away from the axis of the structure. Bias can even be automatic, i.e. the routine automatically calculates the cell size in the radial direction in order to preserve the relationship between the circumferential and radial directions for all cells. The total number of cells that the user wishes to insert in the radial direction does not change.
- Adaptive cells. By activating this option the nodes of all cells follow the inner and outer skin (or frontiers). Therefore, this enables the basic structure of the cells to be modified, while keeping their internal connections unchanged in order to match the extreme nodes of the external cells with those of the skins.

In order to define a specific cell (or to determine the best unit cell in an optimization process), a set of flags has to be defined. By setting the flag parameters appropriately, it is possible to generate unit cells with a different topology. Fig. 4 and Fig. 5 show some examples of 8-node UC and 27-node UC.

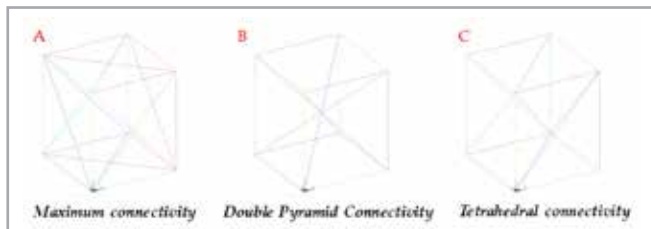


Fig. 4 – Connections in an 8-node Unit Cell. (A) Maximum connectivity UC; (B) Double pyramid connectivity UC; (C) Tetrahedral connectivity UC.

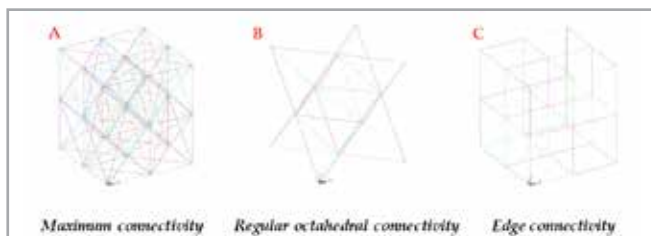


Fig. 5 – Connections in a 27-node Unit Cell. (A) Maximum connectivity UC; (B) Regular octahedral connectivity UC; (C) Edge connectivity UC.

Numerical Applications

The numerical procedure developed allows a lot of axial-symmetric structures to be realized very simply, based on the concept of lattice structures. The lattice structure and the internal skin are always assumed to have been made with additive manufacturing technology,

while the external skin can be made from the same material as the other parts or from composite material.

It goes without saying that the numerical models developed can be used for any kind of numeric analysis. The tool has been designed to replicate different types of loading conditions, but others not currently implemented can easily be introduced. Furthermore, to keep the models fairly inexpensive computationally, all the nodes of all the parts are merged into each other - including the interface nodes between the lattice part and the skins. While this leads to greater complexity during model generation, it makes it possible to avoid the use of bonded contact regions. Hereafter we report some examples to demonstrate the tool's versatility.

Test Case 1

The first test case concerns a truncated conical structure with an internal skin and lattice structure in titanium alloy (electron beam melting process) and an external skin in composite material with the following lamination sequence [45; -45]2. Both skins have a thickness of 1mm, while the diameter of the beams in the lattice structure is 1mm. Fig. 6 shows a schematic of the analyzed structure, the global FE model, the details of the unit cell used, and a section of the internal sub-structure.

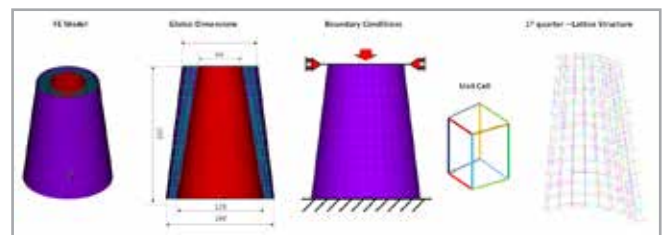


Fig. 6 – Test Case 1: Geometry, boundary conditions, and unit cell selected

An 8-node adaptive cell without a bias factor was used for this structure. The cell has only 12 connections, represented by the edges of the cell and neglecting the diagonal connections. The structure was subjected to a compressive loading condition to evaluate the buckling load using linear buckling analysis. The entire structure weighs 0.609kg, of which 0.246kg relates to the lattice part, 0.099kg to the external composite skin, and 0.262kg to the internal metallic skin.

Fig. 8 shows the nodal displacements (eigenvector) for the first buckling mode (eigenvalue) calculated and highlights the fact that instability involves both the skins and the internal lattice structure. Actually, for both components, local buckling modes were found without global instability that could compromise the load capacity. The critical displacement that generates the first buckling mode is 1.63mm, while the equivalent critical compressive load is 394.02kN.

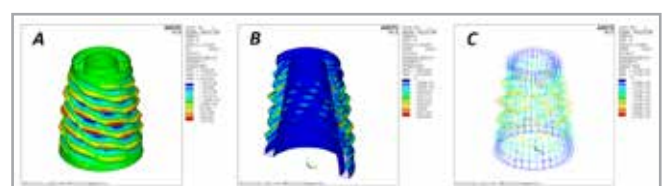


Fig. 7 – Test Case 1: Global displacement at 1st buckling mode. A: Cylindrical reference system; B: Section view; C: Internal lattice structure

■ CASE STUDIES

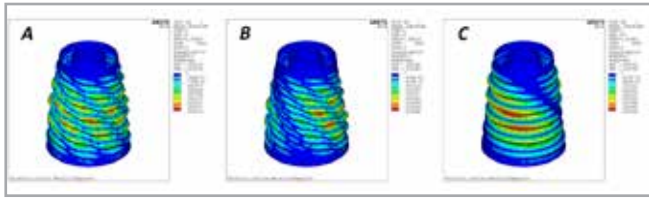


Fig. 8 – Test Case 1: Global displacement relative to buckling modes. A: 2nd mode; B: 5th mode; C: 10th mode

Therefore, the structure can withstand significant compressive loading before buckling occurs.

Fig. 8 shows the nodal displacements (in a cylindrical reference system) for the other buckling modes which can also be classified as local buckling modes.

The results highlight that such a structure is characterized by a large number of very closely spaced local buckling modes, which do not compromise the global loading capabilities [12].

Test Case 2

The second test case involves a cylindrical structure with an external skin in composite material and an internal lattice structure in titanium alloy. The structure's total mass is 157g, of which the lattice structure weighs 98g, and the remaining 58g can be attributed to the external skin. The cylinder was subjected to axial compressive loading conditions.

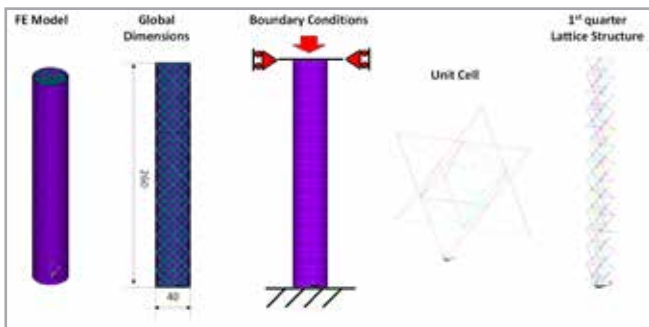


Fig. 9 - Test Case 2: Geometry, boundary conditions, and unit cell adopted

A 27-node Cartesian cell was used for this structure. It has 36 connections and is classified as a regular octahedral. The structure has no internal skin, while the layup of the external skin is [45;-45]₃. The above figure shows the adopted elementary cell and a quarter of the global lattice structure. The numerical results reported show the instability limits, evaluated by means of a static non-linear analysis.

Fig. 10 shows the deformed shape at about 140kN, which corresponds to 10.82mm of applied axial displacement (U₀). As can be seen from the images, this load value triggers local forms of buckling that involve both the skin and the internal beams. These results were also confirmed by linear buckling analyses [12], not reported here for the sake of brevity. As the load increases, more instabilities are triggered, and the structure is unable to withstand further load increments (Fig. 12).

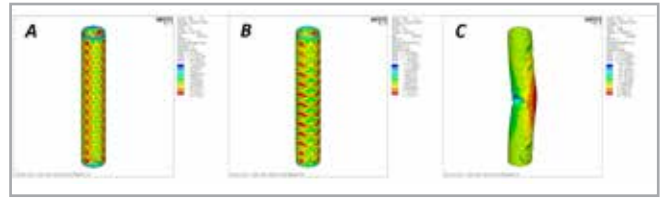


Fig. 10 - Test Case 2: Radial displacement. A: U₀ = 10.8mm; B: U₀ = 13.1mm; C: U₀ = 15.1mm.

The graph in Fig. 11 shows the time history of the reaction load in the axial direction. From this graph it is evident that the global buckling is triggered at about 13mm (applied displacement), which correspond to 162kN. After the first modes of local buckling (140kN), the structure is then able to withstand an additional, fairly constant load of 15% until total collapse occurs at about U₀ = 15mm.

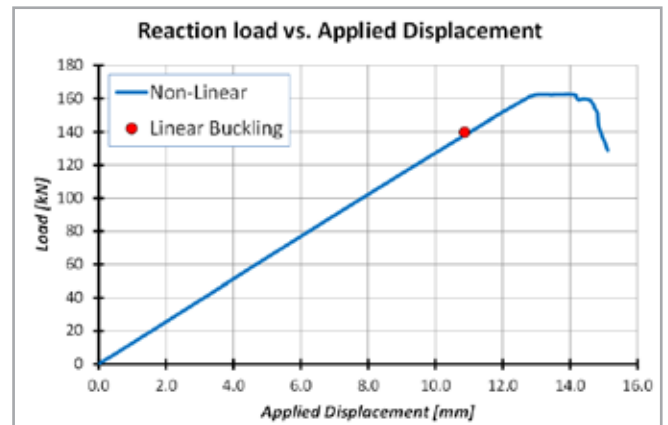


Fig. 11 - Test Case 2: Load vs. applied displacement

Test Case 3

The third test case examines an axisymmetric structure, representing a convergent-divergent nozzle. The applied load distributes a uniform pressure on the inner surface of the inner skin equal to 0.1MPa. The constraints aim to eliminate the concentration of undesired stress and obtain an isostatic structure. Fig. 12 shows the analyzed structure with its dimensions and the applied boundary conditions.

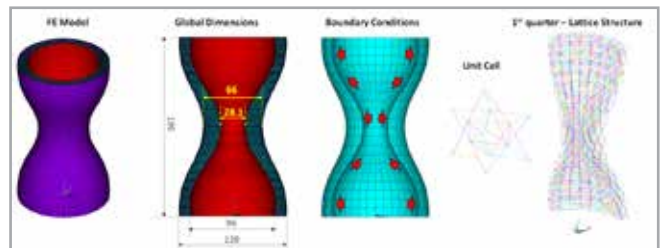


Fig. 12 - Test Case 3: Geometry, boundary conditions, and unit cell adopted.

An adaptive cylindrical cell with 27 nodes was used. The cell has 36 connections and is classified as a regular octahedral. The diameter of each element of the lattice structure is equal to 1.0mm.

The thickness of the metallic inner skin is 0.5mm while the layup of the external skin is [45; -45]₃. The overall structural mass is 486g, consisting of 272g for the lattice structure, 113g for the composite outer skin, and 100g for the metallic inner skin. Fig. 13 shows the

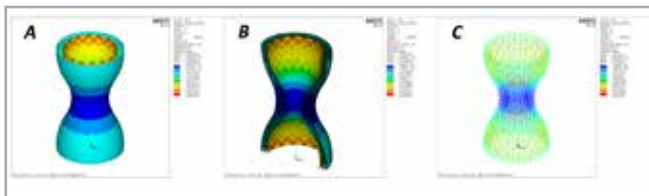


Fig. 13 - Test Case 3: Global displacement. A: Entire model; B: Section view; C: Lattice structure

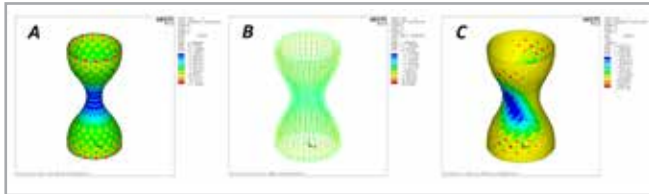


Fig. 14 - Test Case 3: Stress distribution. A: Inner metallic skin; B: Lattice structure; C: Outer composite skin

global displacements of the entire structure and the detail of the internal lattice structure.

The following figures show the stress state of the metal parts, i.e. the internal skin, the internal beams, and the external composite skin. For the internal skin, the Von Mises equivalent stress is reported, while for the beams the axial stress state is reported.

For the external composite skin, the stress in fiber direction is reported for the outer layer (similar data is obviously available for all layers in all directions).

Conclusions

The work briefly describes an automatic procedure based on APDL macros to study complex structures made of lattice structures and solid parts. This procedure also enables the study of hybrid metal/composite structures. Given their complexity, the metal parts are intended to be created with additive manufacturing technologies.

The procedure is able to create axial-symmetric structures with different types of unit cells by simply defining a few parameters. The cells fit perfectly into the structure; therefore, no cuts are made at the boundary surfaces of the inner and outer skins. In order to reduce computational costs, various solutions were implemented: exclusive use of shell and beam elements; connections between parts made by merging the interface nodes and avoiding the use of contact algorithms with bonded option.

The use of this procedure permits many axial symmetric components to be analyzed quickly and simply. In particular, it provides valuable support for studying the performance of lattice structures with and without solid parts and with both metallic and composite material systems. Moreover, the APDL macro, being fully parametrized, enables sensitivity analyses and optimization processes to be performed.

For more information:

Francesco Di Caprio - CIRA Italian Aerospace Research Centre
f.dicaprio@cira.it

References

- Wei Gao, Yunbo Zhang, Devarajan Ramanujan, Karthik Ramani, Yong Chen, Christopher B. Williams, Charlie C.L. Wang, Yung C. Shin, Song Zhang, Pablo D. Zavattieri. The status, challenges, and future of additive manufacturing in engineering, *Computer-Aided Design*, Volume 69, 2015, Pages 65-89.
- Tofail, S.A.; Koumoulos, E.P.; Bandyopadhyay, A.; Bose, S.; O'Donoghue, L.; Charitidis, C. Additive manufacturing: Scientific and technological challenges, market uptake and opportunities. *Materials Today*, 2018, 21(1), 22-37.
- Berman, B. 3-D printing: The new industrial revolution. *Business Horizons*, 2012, 55(2), 155-162.
- Huang, S.H.; Liu, P.; Mokasdar, A.; Hou, L. Additive manufacturing and its societal impact: A literature review. *International Journal of Advanced Manufacturing Technology*, 2013, 67(5-8), 1191-1203.
- Gao, W.; Zhang, Y.; Ramanujan, D.; Ramani, K.; Chen, Y.; Williams, C.B.; Wang, C.C.L.; Shin, Y.C.; Zhang, S.; Zavattieri, P.D. The status, challenges, and future of additive manufacturing in engineering. *CAD Computer Aided Design*, 2015, 69, 65-89.
- Thompson, M.K.; Moroni, G.; Vaneker, T.; Fadel, G.; Campbell, R.I.; Gibson, I.; Bernard, A.; Schulz, J.; Graf, P.; Ahuja, B.; Martina, F. Design for Additive Manufacturing: Trends, opportunities, considerations, and constraints. *CIRP Annals - Manufacturing Technology*, 2016, 65 (2), 737-760.
- Wu, P.; Wang, J.; Wang, X. A critical review of the use of 3-D printing in the construction industry. *Automation in Construction*, 2016, 68, 21-31.
- Panesar, A.; Abdi, M.; Hickman, D.; Ashcroft, I. Strategies for functionally graded lattice structures derived using topology optimisation for additive manufacturing. *Additive Manufacturing*, 2018, 19, 81-94.
- Ngo, T.D.; Kashani, A.; Imbalzano, G.; Nguyen, K.T.Q.; Hui, D. Additive manufacturing (3D printing): A review of materials, methods, applications and challenges. *Composites Part B: Engineering*, 2018, 143, 172-196.
- Yeh, Chin-Ching. "Trend analysis for the market and application development of 3D printing." *International Journal of Automation and Smart Technology* 4.1, 2014, 1-3.
- Dilberoglu, U.M.; Gharehpapagh, B.; Yaman, U.; Dolen, M. The role of additive manufacturing in the era of industry 4.0. *Procedia Manuf*, 2017, 11, 545-554.
- Di Caprio, F.; Acanfora, V.; Franchitti, S.; Sellitto, A.; Riccio, A.; Hybrid Metal/Composite lattice structures: Design for Additive Manufacturing; 2019 Aerospace, 6 (6), art. no. 71.
- Tomlin, Matthew, and Jonathan Meyer. "Topology optimization of an additive layer manufactured (ALM) aerospace part." *Proceeding of the 7th Altair CAE technology conference*, 2011.
- Chen, W.; Zheng, X.; Liu, S. Finite-Element-Mesh Based Method for Modeling and Optimization of Lattice Structures for Additive Manufacturing. *Materials*, 2018, 11, 2073.
- Ferro, C.G.; Varetti, S.; Vitti, F.; Maggiore, P.; Lombardi, M.; Biamino, S.; Manfredi, D.; Calignano, F. A Robust Multifunctional Sandwich Panel Design with Trabecular Structures by the Use of Additive Manufacturing Technology for a New De-Icing System. *Technologies*, 2017, 5, 35.
- WILLIAMS, Christopher B.; COCHRAN, Joe K.; ROSEN, David W. Additive manufacturing of metallic cellular materials via three-dimensional printing. *The International Journal of Advanced Manufacturing Technology*, 2011, 53.1-4: 231-239.
- ROSEN, David W. Computer-aided design for additive manufacturing of cellular structures. *Computer-Aided Design and Applications*, 2007, 4.5: 585-594.
- DESHPANDE, Vikram S.; FLECK, Norman A.; ASHBY, Michael F. Effective properties of the octet-truss lattice material. *Journal of the Mechanics and Physics of Solids*, 2001, 49.8: 1747-1769.
- Ferrigno, A.; Di Caprio, F.; Borrelli, R.; Auricchio, F.; Vigliotti, A. The mechanical strength of Ti-6Al-4V columns with regular octet microstructure manufactured by electron beam melting. *Materialia*, 2019, 5, 100232.
- Deshpande, V.; Fleck, N.; Ashby, M. Effective properties of the octet-truss lattice material. *Journal of the Mechanics and Physics of Solids*, 2001, 49(8), 1747-1769.